Dynamical Singularities of Floquet Higher-Order Topological Insulators

Haiping Hu,[1,2] Biao Huang,[2] Erhai Zhao,[1,3] and W. Vincent Liu[2,4,5]
[1]*Department of Physics and Astronomy, George Mason University, Fairfax, Virginia 22030, USA*
[2]*Department of Physics and Astronomy, University of Pittsburgh, Pittsburgh, Pennsylvania 15260, USA*
[3]*Quantum Materials Center, George Mason University, Fairfax, Virginia 22030, USA*
[4]*Wilczek Quantum Center, School of Physics and Astronomy and T.D. Lee Institute, Shanghai Jiao Tong University, Shanghai 200240, China*
[5]*Shenzhen Institute for Quantum Science and Engineering and Department of Physics, Southern University of Science and Technology, Shenzhen 518055, China*

(Received 16 May 2019; accepted 15 January 2020; published 3 February 2020)

We propose a versatile framework to dynamically generate Floquet higher-order topological insulators by multistep driving of topologically trivial Hamiltonians. Two analytically solvable examples are used to illustrate this procedure to yield Floquet quadrupole and octupole insulators with zero- and/or π-corner modes protected by mirror symmetries. Furthermore, we introduce dynamical topological invariants from the full unitary return map and show its phase bands contain Weyl singularities whose topological charges form dynamical multipole moments in the Brillouin zone. Combining them with the topological index of a Floquet Hamiltonian gives a pair of $\mathbb{Z}_2$ invariant ν_0 and ν_π which fully characterize the higher-order topology and predict the appearance of zero- and π-corner modes. Our work establishes a systematic route to construct and characterize Floquet higher-order topological phases.

DOI: 10.1103/PhysRevLett.124.057001

Introduction.—Topological phases of matter [1,2] are characterized by bulk topological invariants and the appearance of robust edge or surface states. Recently, the notion of topological phases and bulk-edge correspondence has been extended to higher-order topological insulators (HOTIs) [3,4]. A defining characteristic of HOTIs is the emergence of corner modes (CMs) or hinge modes, i.e., excitations at the intersections of edges or surfaces with energies inside the bulk gap and protected by crystalline symmetries [3–18]. Theoretical concepts such as the nested Wilson loops [3,4] and many-body multipole operators [19,20] have been proposed to capture their topological properties and the bulk-corner or hinge correspondence. Experimentally, HOTIs have been observed in phononic [21] and photonic systems [22–24], circuit arrays [25], and crystal solids [26].

The notion of topological phases has also been generalized to Floquet systems where the Hamiltonian is periodic in time, $H(t+T) = H(t)$, with T the driving period [27–31]. Periodic driving provides a powerful tool to engineer the quasienergy band structure by tuning the driving amplitude, frequency, and shape. Despite the apparent similarity between quasienergy and energy, the topological properties of Floquet systems are much richer than static systems. One of its unique features is the appearance of in-gap modes pinned at quasienergy, $\varepsilon = 0, \pi/T$, and localized at the edge, even though the bulk quasienergy bands are trivial. Such anomalous Floquet topological insulators are intrinsically dynamical phases. In order to systematically classify Floquet topological phases [32–34], one must examine the full time-evolution operator $U(t)$. In particular, the so-called return map $\tilde{U}(t)$ [see Eq. (1) below] defines a $\mathbb{Z}$ or $\mathbb{Z}_2$ topological invariant [33,34] for each quasienergy gap. In 2D, for example, it corresponds to the winding number [31,35,36] which counts the topological charge of Weyl-like singularities [37,38] in the instantaneous phase band during time evolution. The return map, together with the effective Hamiltonian H_F, can describe a large class of first-order Floquet topological insulators [32–34].

It is then natural to ask whether periodic driving can give rise to new high-order topological phenomena that have no static analogs, and if so, how to characterize them. Recently, several specific models have appeared to realize Floquet HOTIs (FHOTIs) in periodically driven systems [39–43]. These proposals, however, rely on building-block Hamiltonians with specific lattice structures or symmetries and are therefore not general. Moreover, the existing topological invariants in Refs. [39–43] are supplied in a case-by-case manner, applicable only to a certain specific model or symmetry class. A theory for FHOTIs that can predict the corner modes from bulk invariants constructed from a general $\tilde{U}(t)$ and H_F is still lacking.

Motivated by these considerations, in this Letter we demonstrate a generic route to realize and characterize FHOTIs. The construction does not rely on any specific space-time symmetries of the building-block Hamiltonians. As an example, a 2D model is solved analytically to determine the phase diagram, which contains two Floquet quadrupole topological phases with 0 and π CMs, respectively. Via the decomposition of the unitary evolution, we show that the topology of the quasienergy bands is captured by $\mathbb{Z}_2$ invariant ν_0^F from the nested Wilson loops, while the return maps feature multipole patterns of dynamical singularities: the topological charges of the Weyl-type singularities of $\tilde{U}(t)$ form a quadrupole moment in the Brillouin zone (BZ) at certain instants. Two dynamical invariants n_0, n_π are introduced to count these charges. From ν_0^F and $n_{0,\pi}$, we show that each quasienergy gap is characterized by a $\mathbb{Z}_2$ index ν that predicts the appearance or absence of CMs. The new $\mathbb{Z}_2$ invariants work for all mirror-symmetry protected FHOTIs and go beyond the periodic table of first-order Floquet topological insulators. The construction and topological analysis are then generalized to 3D Floquet octupole topological insulators.

Dynamical construction of FHOTI.—The dynamics of a periodically driven lattice system with Hamiltonian $H(t)$ is governed by the unitary evolution $U(t) = \mathcal{T} e^{-i\int_0^t H(\tau)d\tau}$, where $\hbar = 1$ and $\mathcal{T}$ denotes time ordering. To extract its topology, it is convenient to decompose $U(t)$ into a unitary loop $\tilde{U}(t)$ satisfying $\tilde{U}(0) = \tilde{U}(T) = I$ and the time evolution of a constant Hamiltonian H_F [33]. Explicitly, one can define the effective Hamiltonian $H_F = i \log U(T)/T$ as well as the return map [31,33,34]:

$$\tilde{U}(t) = U(t)e^{iH_F t}. \tag{1}$$

Usually, $\tilde{U}(t)$ is defined for a given gap with the logarithm branch cut lying within it. It is apparent from Eq. (1) that the topology of $U(t)$ is carried by both H_F and $\tilde{U}(t)$. The spectra ε_n of H_F are known as quasienergy bands, and we take $\varepsilon_n \in [-\pi/T, \pi/T]$.

The basic idea of dynamical construction of FHOTIs can be illustrated by a simple example of a Floquet quadrupole insulator depicted in Fig. 1(a). Consider a square lattice, where each unit cell (shaded box) consists of four lattice sites. Our strategy is to herd the motion (more precisely, the quantum walks) of particles by spatial control of the tunneling amplitudes in multiple steps within each driving period. Three trivial Hamiltonians, h_x, h_y, and h_0, serve as the building blocks: $h_{x/y}$ only contains intercell hopping $t_{x/y}$ along the x/y direction, and h_0 only contains intracell hopping t_0. To visualize the emergence of topological CMs, consider the limit of $t_0 = 0$ and two-step driving: $H(t < T/2) = h_y$ followed by $H(t > T/2) = h_x$. The semiclassical particle motion is sketched in Fig. 1(b). It is clear that particles in the bulk move along a plaquette, while particles on the four edges hop back and forth. However, particles initially at the four corners remain localized and completely decoupled from the bulk and edge dynamics. They are nothing but Floquet CMs. We will show below that the CMs persist to finite t_0 as the bulk excitations form Floquet bands separated by gaps. Similar to the static case [3,4], the Floquet CM is protected by crystalline symmetries (e.g., mirror reflection).

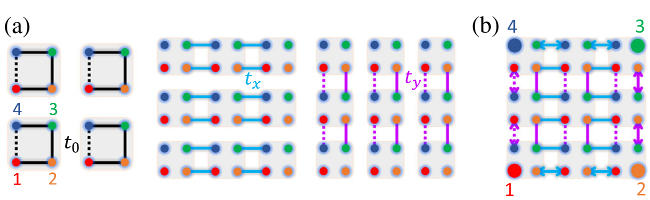

FIG. 1. Construction of a FHOTI on a square lattice from multistep driving. (a) The trivial building blocks h_0 (left), h_x (middle), and h_y (right) with intracell hopping t_0 and intercell hopping t_x, t_y. Dashed lines represent hoppings with negative signs. (b) Schematic of particle motion in one period of two-step driving h_y followed by h_x with $t_0 = 0$. The corners are dynamically decoupled from the bulk, giving rise to four localized corner modes (big solid circles).

This picture motivates us to propose the following generic N-step driving sequence. In each step s with time interval T_s the system evolves according to a constant Hamiltonian h_s assumed, for simplicity, to be a sum of anticommuting terms [see h_0, $h_{x,y}$ in Eq. (4) below]. Accordingly,

$$U(T) = \prod_{s=1}^{N} (\cos\theta_s - i \sin\theta_s \tilde{h}_s). \tag{2}$$

Here, $\theta_s = T_s|E_s|$, $\tilde{h}_s = h_s/|E_s|$, with $\pm E_s$ the spectrum of h_s. By definition, the wave functions of CMs at quasienergy zero (0 CM) and π/T (πCM) satisfy

$$U(T)|\psi_0\rangle = |\psi_0\rangle, \qquad U(T)|\psi_\pi\rangle = -|\psi_\pi\rangle. \tag{3}$$

The existence of a solution to these eigenequations is guaranteed by properly choosing θ_s and h_s as follows. Consider a state $|\eta\rangle$ localized at the corner [Fig. 1(b)]. It may couple to neighboring sites by $h_{s=1}$ in the first step, but for all other steps $s > 1$, h_s is chosen, so $h_{s>1}|\eta\rangle = 0$. A 0 CM is realized if we choose $\theta_1 = 0$. Its wave function $|\psi_0\rangle$ is simply given by $|\eta\rangle$. Similarly setting $\theta_1 = \pi$ gives rise to πCM with $|\psi_\pi\rangle = |\eta\rangle$. For 0 and π CMs to coexist [39], one can choose, for example, $\theta_1 = \pi/2$ and $\theta_{s>1} = \pi$ for even N. We will give a few examples below to illustrate how this construction procedure can be applied to generate different kinds of FHOTIs.

Floquet quadrupole insulator.—First, we present an analytically solvable model of the Floquet quadrupole insulator (FQI) and demonstrate the emergence of topological CMs. The overall setup has been introduced in Fig. 1 on the square lattice. The 2×2 unit cell is conveniently described by two sets of Pauli matrices $\boldsymbol{\sigma}$ and $\boldsymbol{\tau}$. The trivial building blocks are hopping Hamiltonians, $h_0 = t_0(\tau_0\sigma_1 + \tau_2\sigma_2)$, $h_x = t_x(\cos k_x \tau_0\sigma_1 - \sin k_x \tau_3\sigma_2)$, and $h_y = t_y(\cos k_y \tau_2\sigma_2 + \sin k_y \tau_1\sigma_2)$, where $\boldsymbol{k} = (k_x, k_y)$ is the quasimomentum. The terms in $h_{0,x,y}$

anticommute and the system possesses two mirror symmetries $\mathcal{M}_x = i\tau_3\sigma_1$ and $\mathcal{M}_y = i\tau_1\sigma_1$. The driving protocol is

$$\begin{aligned} &t \in T_1, H(t) = h_0, \qquad t \in T_2, H(t) = h_y, \\ &t \in T_3, H(t) = h_x, \qquad t \in T_4, H(t) = h_0, \end{aligned} \tag{4}$$

with time interval $T_s = [(s-1)T/4, sT/4)$. For $t_x T = t_y T = \pi$, the FQI phase with 0 CMs appears when [44]

$$(\mathcal{N} - 1/6)\pi < \phi_0 < (\mathcal{N} + 1/6)\pi, \qquad \mathcal{N} \in \mathbb{Z}, \tag{5}$$

with $\phi_0 \equiv (t_0 T/2\sqrt{2})$. The FQI phase with π CMs lies within

$$(\mathcal{N} + 1/3)\pi < \phi_0 < (\mathcal{N} + 2/3)\pi, \qquad \mathcal{N} \in \mathbb{Z}. \tag{6}$$

For all other values of ϕ_0, the system is a trivial band insulator with no CMs.

Figure 2(a) shows the quasienergy spectra as a function of ϕ_0 for a finite lattice with open boundary conditions. In between the bulk bands, we observe fourfold degenerate in-gap modes pinned at $\varepsilon = 0$ or $\varepsilon = \pi/T$. They appear alternatively with a period of exactly π as ϕ_0 is varied, and are separated from each other by the topologically trivial phase, consistent with Eqs. (5) and (6). The wave functions of these in-gap modes are shown in Fig. 2(b). They are indeed localized at the four corners arising from the bulk quadrupoles. In comparison, the quasienergy spectra for periodic boundary condition or stripe geometry are fully gapped [44], indicating vanishing conventional dipoles.

This model provides an elegant example of our dynamical construction of FHOTIs and CMs summarized in Eq. (2). Denote the wave functions of four CMs as $|\psi^i_{0/\pi}\rangle$ $(i = ll, lr, ul, ur)$ and take $i = ll$, the lower-left corner, for example. For $\phi_0 = 0$, the 0-CM wave function is localized at a single site labeled as 1 (Fig. 1),

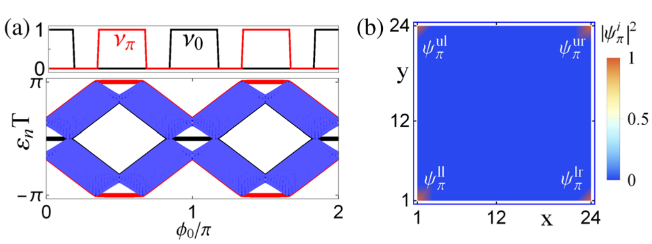

FIG. 2. (a) Phase diagram of the Floquet system with driving Eq. (4). Top: Topological invariants ν_0 (black) and ν_π (red) obtained from Eq. (9) showing two FQI phases. Bottom: Quasienergy spectra for a finite 24×24 lattice. The fourfold degenerate 0 (π) CMs are marked by the black (red) lines. (b) The spatial wave functions of four π CMs, $|\psi^i_\pi|^2 (i = ll, lr, ul, ur)$, $\phi_0/\pi = 0.45$, $t_x = t_y = \pi/T$.

$|\psi^{ll}_0\rangle = |1\rangle_{ll}$, corresponding to the value $\theta_1 = 0$ in our construction scheme. The other two driving steps $h_{x,y}$ do not couple the CMs to the bulk. For $\phi_0 = \pi/2$, the π-CM wave function is $|\psi^{ll}_\pi\rangle = (1/\sqrt{2})(|2\rangle_{ll} - |4\rangle_{ll})$, corresponding to $\theta_1 = \pi$. When deviating from these ideal limits, the CMs spread further into the bulk but remain localized. The FQI and CMs persist as long as the bulk gaps stay open.

Dynamical topological invariants.—For static HOTIs, the higher-order bulk topology and appearance of CMs can be described by introducing Wannier bands and nested Wilson loops [3,4,44,45]. The analysis can be generalized to Floquet systems to capture the topological properties of H_F and the quasienergy bands. We chose the lower two overlapping quasienergy bands to construct the Wannier-band subspace $|\omega^j_{x,\boldsymbol{k}}\rangle$ $(j = 1, 2)$ and compute the nested polarizations [3,4,44], for example,

$$p^j_y = i \int_{\mathrm{BZ}} \frac{d^2k}{(2\pi)^2} \langle \omega^j_{x,\boldsymbol{k}} | \partial_{k_y} | \omega^j_{x,\boldsymbol{k}} \rangle. \tag{7}$$

In the presence of mirror symmetries $\mathcal{M}_x$ and $\mathcal{M}_y$, the nested polarizations p^j_y and p^j_x are quantized to be 0 (trivial) or 1/2 (topological) [3,4], yielding a $\mathbb{Z}_2$ classification. The topological quadrupole phase corresponds to $(p^j_y, p^j_x) = (1/2, 1/2)$. It is characterized by $\mathbb{Z}_2$ invariant

$$\nu^F_0 = 4 p^j_y p^j_x. \tag{8}$$

For the two FQI phases above, ν^F_0 is found to be 1, which is consistent with the quantized tangential polarization along the edges [3,4,44]. By itself, however, ν^F_0 cannot distinguish the two FQI phases or predict in which gap the CMs reside or even the existence of CMs (e.g., for anomalous FQI [39], ν^F_0 is zero but CMs are present). This is not surprising because it only captures the topology of H_F, not the full $U(t)$. For FHOTI, an intrinsically dynamical topological invariant is needed.

Such a dynamical invariant can be defined from the return map $\tilde{U}(t)$. The diagonalization of $\tilde{U}$ yields $\tilde{U}(t) = \sum_m e^{-i\tilde{\varepsilon}_m(\boldsymbol{k},t)} |\varphi_m(\boldsymbol{k},t)\rangle\langle\varphi_m(\boldsymbol{k},t)|$, with the eigenphases $\tilde{\varepsilon}_m$ forming the phase bands [33,37]. For our system, during the time evolution $t \in (0, T)$, the gap may close at 0 or π/T as the phase bands touch each other at isolated points in the $(\boldsymbol{k}, t)$ space, similar to Weyl points in semimetals, and reopen afterwards. Such singular points resemble magnetic monopoles and carry topological charges [37]. For the ith degeneracy point $\boldsymbol{d}_j = (\boldsymbol{k}_j, t_j)$ of band m, we compute its topological charge, $C_j = (1/2\pi i) \oint_{\boldsymbol{S}_j} \boldsymbol{\nabla} \times \langle \varphi_m(\boldsymbol{k},t) | \boldsymbol{\nabla} | \varphi_m(\boldsymbol{k},t) \rangle \cdot d\boldsymbol{S}$, with $\boldsymbol{S}_j$ a small surface enclosing $\boldsymbol{d}_j$.

Because of the mirror symmetries $\mathcal{M}_{x,y}$, these "Weyl points" at a specific time instant always come in quartets, i.e., at $\boldsymbol{k} = (\pm k_x, \pm k_y)$ in the 2D BZ. And their

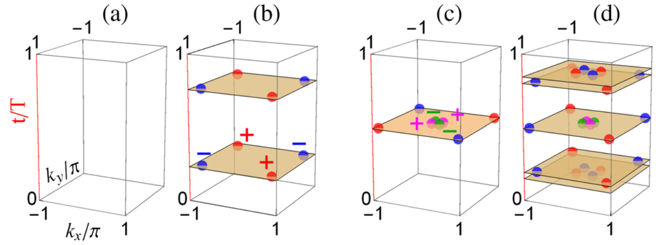

FIG. 3. Dynamical singularities of FQIs in $(\boldsymbol{k}, t)$ space. The colored dots label the Weyl charges in the phase band of $\tilde{U}(t)$ at certain time instants. Their topological charges form quadrupole moments in the BZ. The red and blue dots label charge ± 1 at the π gap; the magenta and green dots label charge ± 1 at the 0 gap. From (a) to (d), $\phi_0/\pi = 0.1, 0.95, 0.45, 1.45$, with $t_x = t_y = \pi/T$.

charges form a quadrupole pattern [46], as illustrated in Figs. 3(a)–3(d). Such a dynamical quadrupole (with zero total charge) indicates the higher-order topology and the absence of 1D edge states [31,37]. In fact, one can prove that a quadrupole pattern is equivalent to its mirror image by a continuous deformation based on $\mathcal{M}_x$ or $\mathcal{M}_y$ [44]. Thus, $n_{0,\pi} = \sum_{\boldsymbol{k}_j \in 1\,\mathrm{st\,qBz}}^{\tilde{\varepsilon}(\boldsymbol{d}_j)=0,\pi} C_j$, the total Weyl charge within the first quadrant of the BZ during $t \in (0, T)$, is only defined modulo 2, and its parity can serve as the dynamical invariant for the corresponding gap. Combining $n_{0,\pi}$ from $\tilde{U}(t)$ with the quadrupole invariant ν_0^F for H_F, we arrive at two $\mathbb{Z}_2$-valued invariants $\nu_{0,\pi}$ for the 0 and π gap, respectively (for details, see Ref. [44]):

$$\nu_\pi = n_\pi \mod 2, \qquad \nu_0 = (n_0 + \nu_0^F) \mod 2. \quad (9)$$

We stress that the $\mathbb{Z}_2$ nature of $\nu_{0,\pi}$ originates from mirror symmetries. A nonzero value of $\nu_0 = 1$ ($\nu_\pi = 1$) indicates the appearance of CMs at the 0 gap (π gap). Thus, our Floquet system follows a $\mathbb{Z}_2 \times \mathbb{Z}_2$ classification and is described by two $\mathbb{Z}_2$ invariants (ν_0, ν_π), one for each gap. To check the correspondence between bulk invariants Eq. (9) and the CMs observed in numerics, we give a few examples of the Weyl charges in Figs. 3(a)–3(d). For the FQI phase with 0 CMs [Figs. 3(a) and 3(b)], we have $n_0 = 0$ and $n_\pi = 0$ or 2. In both cases, $(\nu_0, \nu_\pi) = (1, 0)$. For the FQI phase with π CMs [Figs. 3(c) and 3(d)], $n_0 = 1$ and $n_\pi = 1$ or 5. Thus, $(\nu_0, \nu_\pi) = (0, 1)$. It is clear that Eq. (9) correctly predicts the appearance of Floquet CMs, in agreement with Fig. 2(a). We have checked that the invariants $\nu_{0,\pi}$ also apply to anomalous FQIs with $\nu_0 = \nu_\pi = 1$ discussed in Refs. [39,44].

Floquet octupole insulator.—Next we show how to generate Floquet octupole insulators (FOIs) on a cubic lattice following our general scheme. The degrees of freedom inside the eight-site unit cell, illustrated in Fig. 4(a), can be described by three sets of Pauli matrices $\boldsymbol{\tau}$, $\boldsymbol{\sigma}$, and $\boldsymbol{s}$. The dynamical construction employs four building blocks: an intraunit cell hopping Hamiltonian,

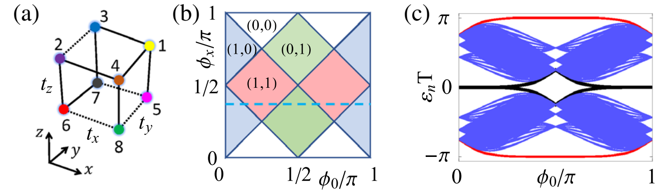

FIG. 4. Floquet octupole insulator. (a) The unit cell contains 8 sites on a cubic lattice, the solid (dashed) lines denote hoppings with + (−) signs. (b) The phase diagram with ϕ_0 and ϕ_x defined in the main text. Color-coded regions represent three FOI phases with 0 CMs only (blue), π CMs only (green), both 0 and π CMs (red), and the trivial phase (white). Each phase is labeled by its dynamical invariants (ν_0, ν_π). (c) Quasienergy spectra of a $16 \times 16 \times 16$ lattice along the dash line in (b) for fixed $\phi_x/\pi = 3/8$. The black (red) lines mark the eightfold degenerate 0 (π) CMs.

$h_0 = t_0(\Gamma_2 + \Gamma_4 + \Gamma_6)$, and three interunit cell hopping Hamiltonians, $h_x = t_x(\sin k_x \Gamma_3 + \cos k_x \Gamma_6)$, $h_y = t_y(\sin k_y \Gamma_1 + \cos k_y \Gamma_2)$, $h_z = t_z(\sin k_z \Gamma_5 + \cos k_z \Gamma_4)$, with $\Gamma_0 = \tau_3\sigma_3 s_0$, $\Gamma_i = -\tau_3\sigma_2 s_i$ for $i = 1, 2, 3$, $\Gamma_4 = \tau_1\sigma_0 s_0$, $\Gamma_5 = \tau_2\sigma_0 s_0$, and $\Gamma_6 = i\prod_{j=0}^{5}\Gamma_j$. The driving protocol consist of two steps: for $0 < t < T/4$ and $3T/4 < t < T$, $H(t) = h_0$; for $T/4 < t < 3T/4$, $H(t) = h_x + h_y + h_z$. Let us focus on the simple case of $t_x = t_y = t_z$. Then the phase boundaries can be found analytically [44],

$$\phi_0 \pm \phi_x = \mathcal{N}\pi/2, \qquad \mathcal{N} \in \mathbb{Z}, \quad (10)$$

with $\phi_0 = \sqrt{3}t_0 T/4$ and $\phi_x = \sqrt{3}t_x T/4$.

The phase diagram on the $\phi_0 - \phi_x$ plane is depicted in Fig. 4(b). It contains three distinct FOIs and a trivial phase. Roughly speaking, the FOI phase with only 0 CMs is located near $\phi_0 = 0$ and π, while the FOI phase with only π CMs occupies regions around $\phi_0 = \pi/2$. Sandwiched in between is the third, anomalous FOI, which has both 0 and π CMs. The quasienergy spectrum for a finite system with open boundary conditions is shown in Fig. 4(c) for parameters along a cut in the phase diagram with fixed $\phi_x = 3\pi/8$. The location of different Floquet CMs agrees with the phase boundaries given by Eq. (10). To cast this example in the general scheme Eq. (2), we notice the 0 CM at point $\phi_0 = 0$ is simply $|\psi_0\rangle = |6\rangle$ with $\theta_1 = 0$. The πCM at $\phi_0 = \pi/2$ is just $|\psi_\pi\rangle = (|2\rangle + |7\rangle - |8\rangle)/\sqrt{3}$ with $\theta_1 = \pi$. The system has three mirror symmetries: $\mathcal{M}_x = \tau_0\sigma_1 s_3$, $\mathcal{M}_y = \tau_0\sigma_1 s_1$, and $\mathcal{M}_z = \tau_0\sigma_3 s_0$. Together they quantize the octupole moment. Similar to the FQIs, the topology of the Floquet system is carried by both H_F and the return map $\tilde{U}(t)$. The former is characterized by a $\mathbb{Z}_2$ invariant ν_0^F [44]; the latter contains singularities of the phase bands in 4D $(\boldsymbol{k}, t)$ space. We find that the invariants in Eq. (9) are still valid [44].

Outlook.—We have introduced a versatile route to construct and characterize FHOTIs. The building blocks are topologically trivial and accessible in many synthetic (e.g., photonic and cold-atoms) quantum systems. For example, the quadrupole phase can be realized based on the π-flux Hofstadter model [47,48] with the addition of a superimposed superlattice along both the x and y directions [3]. Alternatively, the modulation along one direction may be replaced by utilizing spin degrees of freedom, with the effective hoppings being induced by Raman coupling and laser-assisted tunneling in different directions, respectively. The driving protocol can be viewed more generally as discrete-time quantum walks on a lattice [49–51]. By imposing further constraints on the building blocks or the driving protocols, our construction can be generalized to realize higher-order topological phases in other symmetry classes. In contrast to previous constructions of model-dependent topological invariants, the phase-band singularities are general for Floquet systems, hinting at the possibility of a unified scheme for characterizing the higher-order topology for a wide class of systems. Experimentally, in addition to the observation of CMs, the higher-order topology may be identified from the tomography of band-touching singularities [52]. Finally, it would be interesting to investigate FHOTIs in the frequency domain [31,53] and the time evolution of CMs from the entanglement perspective [44].

This work is supported by NSF Grant No. PHY-1707484 (H. H. and E. Z.), AFOSR Grant No. FA9550-16-1-0006 (H. H., E. Z., and W. V. L.), MURI-ARO Grant No. W911NF-17-1-0323 (B. H. and W. V. L.), and NSF of China Overseas Scholar Collaborative Program Grant No. 11429402 sponsored by Peking University (W. V. L.).

[1] M. Z. Hasan and C. L. Kane, Colloquium: Topological insulators, Rev. Mod. Phys. **82**, 3045 (2010).
[2] X.-L. Qi and S.-C. Zhang, Topological insulators and superconductors, Rev. Mod. Phys. **83**, 1057 (2011).
[3] W. A. Benalcazar, B. A. Bernevig, and T. L. Hughes, Quantized electric multipole insulators, Science **357**, 61 (2017).
[4] W. A. Benalcazar, B. A. Bernevig, and T. L. Hughes, Electric multipole moments, topological multipole moment pumping, and chiral hinge states in crystalline insulators, Phys. Rev. B **96**, 245115 (2017).
[5] J. Langbehn, Y. Peng, L. Trifunovic, F. von Oppen, and P. W. Brouwer, Reflection-Symmetric Second-Order Topological Insulators and Superconductors, Phys. Rev. Lett. **119**, 246401 (2017).
[6] Z. Song, Z. Fang, and C. Fang, $d-2$)-Dimensional Edge States of Rotation Symmetry Protected Topological States, Phys. Rev. Lett. **119**, 246402 (2017).
[7] F. Schindler, A. M. Cook, M. G. Vergniory, Z. Wang, S. S. P. Parkin, B. A. Bernevig, and T. Neupert, Higher-order topological insulators, Sci. Adv. **4**, eaat0346 (2018).
[8] F. K. Kunst, G. van Miert, and E. J. Bergholtz, Lattice models with exactly solvable topological hinge and corner states, Phys. Rev. B **97**, 241405(R) (2018).
[9] Q. Wang, C.-C. Liu, Y.-M. Lu, and F. Zhang, High-Temperature Majorana Corner States, Phys. Rev. Lett. **121**, 186801 (2018).
[10] Z. Yan, F. Song, and Z. Wang, Majorana Corner Modes in a High-Temperature Platform, Phys. Rev. Lett. **121**, 096803 (2018).
[11] L. Trifunovic and P. W. Brouwer, Higher-Order Bulk-Boundary Correspondence for Topological Crystalline Phases, Phys. Rev. X **9**, 011012 (2019).
[12] D. Călugăru, V. Juričić, and B. Roy, Higher-order topological phases: A general principle of construction, Phys. Rev. B **99**, 041301(R) (2019).
[13] M. Ezawa, Higher-Order Topological Insulators and Semimetals on the Breathing Kagome and Pyrochlore Lattices, Phys. Rev. Lett. **120**, 026801 (2018).
[14] M. Geier, L. Trifunovic, M. Hoskam, and P. W. Brouwer, Second-order topological insulators and superconductors with an order-two crystalline symmetry, Phys. Rev. B **97**, 205135 (2018).
[15] B.-Y. Xie, H.-F. Wang, H.-X. Wang, X.-Y. Zhu, J.-H. Jiang, M.-H. Lu, and Y.-F. Chen, Second-order photonic topological insulator with corner states, Phys. Rev. B **98**, 205147 (2018).
[16] L. Li, M. Umer, and J. Gong, Direct prediction of corner state configurations from edge winding numbers in two- and three-dimensional chiral-symmetric lattice systems, Phys. Rev. B **98**, 205422 (2018).
[17] X.-W. Luo and C. Zhang, Higher-Order Topological Corner States Induced by Gain and Loss, Phys. Rev. Lett. **123**, 073601 (2019).
[18] S. A. A. Ghorashi, X. Hu, T. L. Hughes, and E. Rossi, Second-order Dirac superconductors and magnetic field induced Majorana hinge modes, Phys. Rev. B **100**, 020509(R) (2019).
[19] B. Kang, K. Shiozaki, and G. Y. Cho, Many-body order parameters for multipoles in solids, Phys. Rev. B **100**, 245134 (2019).
[20] W. A. Wheeler, L. K. Wagner, and T. L. Hughes, Many-body electric multipole operators in extended systems, Phys. Rev. B **100**, 245135 (2019).
[21] M. Serra-Garcia, V. Peri, R. Süsstrunk, O. R. Bilal, T. Larsen, L. G. Villanueva, and S. D. Huber, Observation of a phononic quadrupole topological insulator, Nature (London) **555**, 342 (2018).
[22] C. W. Peterson, W. A. Benalcazar, T. L. Hughes, and G. Bahl, A quantized microwave quadrupole insulator with topologically protected corner states, Nature (London) **555**, 346 (2018).
[23] A. Hassan, F. Kunst, A. Moritz, G. Andler, E. Bergholtz, and M. Bourennane, Corner states of light in photonic waveguides, Nat. Photonics **13**, 697 (2019).
[24] S. Mittal, V. V. Orre, G. Zhu, M. A. Gorlach, A. Poddubny, and M. Hafezi, Photonic quadrupole topological phases, Nat. Photonics **13**, 692 (2019).
[25] S. Imhof, C. Berger, F. Bayer, J. Brehm, L. Molenkamp, T. Kiessling, F. Schindler, C. H. Lee, M. Greiter, T. Neupert, and R. Thomale, Topolectrical circuit realization of topological corner modes, Nat. Phys. **14**, 925 (2018).
[26] F. Schindler *et al.*, Higher-order topology in bismuth, Nat. Phys. **14**, 918 (2018).

[27] J. Cayssol, B. Dra, F. Simon, and R. Moessner, Floquet topological insulators, Phys. Status Solidi RRL **7**, 101 (2013).

[28] L. Jiang, T. Kitagawa, J. Alicea, A. R. Akhmerov, D. Pekker, G. Refael, J. I. Cirac, E. Demler, M. D. Lukin, and P. Zoller, Majorana Fermions in Equilibrium and in Driven Cold-Atom Quantum Wires, Phys. Rev. Lett. **106**, 220402 (2011).

[29] N. H. Lindner, G. Refael, and V. Galitski, Floquet topological insulator in semiconductor quantum wells, Nat. Phys. **7**, 490 (2011).

[30] T. Kitagawa, E. Berg, M. Rudner, and E. Demler, Topological characterization of periodically driven quantum systems, Phys. Rev. B **82**, 235114 (2010).

[31] M. S. Rudner, N. H. Lindner, E. Berg, and M. Levin, Anomalous Edge States and the Bulk-Edge Correspondence for Periodically Driven Two-Dimensional Systems, Phys. Rev. X **3**, 031005 (2013).

[32] M. Fruchart, Complex classes of periodically driven topological lattice systems, Phys. Rev. B **93**, 115429 (2016).

[33] R. Roy and F. Harper, Periodic table for Floquet topological insulators, Phys. Rev. B **96**, 155118 (2017).

[34] S. Yao, Z. Yan, and Z. Wang, Topological invariants of Floquet systems: General formulation, special properties, and Floquet topological defects, Phys. Rev. B **96**, 195303 (2017).

[35] Z. Zhou, I. I. Satija, and E. Zhao, Floquet edge states in a harmonically driven integer quantum Hall system, Phys. Rev. B **90**, 205108 (2014).

[36] M. Lababidi, I. I. Satija, and E. Zhao, Counter-Propagating Edge Modes and Topological Phases of a Kicked Quantum Hall System, Phys. Rev. Lett. **112**, 026805 (2014).

[37] F. Nathan and M. S. Rudner, Topological singularities and the general classification of Floquet-Bloch systems, New J. Phys. **17**, 125014 (2015).

[38] E. Zhao, Anatomy of a periodically driven p-wave superconductor, Z. Naturforsch. A **71**, 883 (2016).

[39] B. Huang and W. V. Liu, Higher-order floquet topological insulators with anomalous corner states, arXiv:1811.00555.

[40] M. Rodriguez-Vega, A. Kumar, and B. Seradjeh, Higher-order Floquet topological phases with corner and bulk bound states, Phys. Rev. B **100**, 085138 (2019).

[41] R. W. Bomantara, L. Zhou, J. Pan, and J. Gong, Coupled-wire construction of static and Floquet second-order topological insulators, Phys. Rev. B **99**, 045441 (2019).

[42] Y. Peng and G. Refael, Floquet Second-Order Topological Insulators from Nonsymmorphic Space-Time Symmetries, Phys. Rev. Lett. **123**, 016806 (2019).

[43] R. Seshadri, A. Dutta, and D. Sen, Generating a second-order topological insulator with multiple corner states by periodic driving, Phys. Rev. B **100**, 115403 (2019).

[44] See Supplemental Material at http://link.aps.org/supplemental/10.1103/PhysRevLett.124.057001 for details on the derivations of $U(T)$, Floquet spectra under different boundary conditions, nest Wilson loop approach, $\mathbb{Z}_2$ invariants, phase-band characterizations of anomalous FQIs and FOIs, and time evolution of CMs.

[45] L. Fidkowski, T. S. Jackson, and I. Klich, Model Characterization of Gapless Edge Modes of Topological Insulators Using Intermediate Brillouin-Zone Functions, Phys. Rev. Lett. **107**, 036601 (2011).

[46] The four "Weyl" charges may merge together by additional symmetries and form a multifold degenerate band singularity at the high-symmetry point. In this case, we can directly count n_0, n_π as the times of multifold band touchings in Eq. (9). A multifold band touching will split into four Weyl charges by small perturbations preserving mirror symmetries.

[47] M. Aidelsburger, M. Atala, M. Lohse, J. T. Barreiro, B. Paredes, and I. Bloch, Realization of the Hofstadter Hamiltonian with Ultracold Atoms in Optical Lattices, Phys. Rev. Lett. **111**, 185301 (2013).

[48] H. Miyake, G. A. Siviloglou, C. J. Kennedy, W. C. Burton, and W. Ketterle, Realizing the Harper Hamiltonian with Laser-Assisted Tunneling in Optical Lattices, Phys. Rev. Lett. **111**, 185302 (2013).

[49] Y. Aharonov, L. Davidovich, and N. Zagury, Quantum random walks, Phys. Rev. A **48**, 1687 (1993).

[50] M. Karski, L. Förster, J.-M. Choi, A. Steffen, W. Alt, D. Meschede, and A. Widera, Quantum walk in position space with single optically trapped atoms, Science **325**, 174 (2009).

[51] T. Kitagawa, M. S. Rudner, E. Berg, and E. Demler, Exploring topological phases with quantum walks, Phys. Rev. A **82**, 033429 (2010).

[52] F. N. Ünal, B. Seradjeh, and A. Eckardt, How to Directly Measure Floquet Topological Invariants in Optical Lattices, Phys. Rev. Lett. **122**, 253601 (2019).

[53] I. Mondragon-Shem, I. Martin, A. Alexandradinata, and M. Cheng, Quantized frequency-domain polarization of driven phases of matter, arXiv:1811.10632v2.